


EFFECTS OF ADDITION OF TRANSITION METALS ON INTERMETALLIC PRECIPITATION IN Al-2%Cu-1%Si-BASED ALLOYS

A. I. Ibrahim , E. M. Elgallad, A. M. Samuel, and F. H. Samuel

Département des Sciences appliquées, Université du Québec à Chicoutimi, Chicoutimi, QC, Canada

H. W. Doty

General Motors Materials Engineering, Pontiac, MI, USA

Copyright © 2017 American Foundry Society
<https://doi.org/10.1007/s40962-017-0196-x>

Abstract

Thermal analysis of various Al-2%Cu-1%Si alloy melts containing different transition metal additions was carried out to determine the sequence of reactions and phases formed during solidification under close-to-equilibrium cooling conditions. The main reactions observed in the base B0 alloy comprised (i) formation of the α -Al dendritic network at 640 °C, followed by precipitation of (ii) α -iron $Al_{15}(Fe,Mn)_3Si_2$ phase at 620 °C and (iii) Al_2Cu and $Al_5Mg_8Si_6Cu_2$ phases simultaneously as the final reaction at 495 °C. Two more reactions were observed with the addition of Zr, V and Ni to the base alloy, in addition to Mg_2Si and $AlSiTiZr$, $AlVTi$, $AlCuNi$ and $AlCuNiFe$ phases. The addition of Mn (0.8%) resulted in reducing the

detrimental effects of the platelet-like morphology of the β - Al_5FeSi iron intermetallic phase by replacing it with the more compact and hence less harmful script-like α - $Al_{15}(Fe,Mn)_3Si_2$ phase and sludge particles. Rare earth metals have an affinity to react with certain transition metals, in particular Cu. The results reported in this study were supported by EDS, WDS and DSC analysis.

Keywords: aluminum alloys, thermal analysis, optical metallography, EPMA, EDS and WDS systems, DSC analysis

Introduction

Adding copper (Cu) to aluminum alloys has many positive benefits which enhance the mechanical properties. First, it increases the alloy strength at both room and high temperatures whether these alloys are heat treated after casting or not. However, it was found that the addition of copper to aluminum reduces corrosion resistance. Magnesium (Mg) is added to aluminum alloys in order to increase the strength and corrosion resistance, and to enhance their weldability. In addition, Mg increases the hardness of Al-Cu alloys, especially in castings, however, with a decrease in the ductility and impact resistance. Even small amounts of Mg can have a profound effect on age hardening.¹⁻⁵ Tavitas-Medrano et al.⁶ reported that small additions of 0.4 weight percent of Mg increase the response of the alloy to artificial aging, thereby increasing the achievable tensile strength and micro-hardness values, however, at the expense of reduced elongation and impact toughness.

In addition to Cu, the addition of transition elements such as nickel (Ni) is considered to be effective for increasing the room- and the high-temperature strength of cast Al-Si alloys by forming stable aluminides.⁷ As with the as-cast condition, the ductility of alloys aged to a T6 temper decreases gradually as the Cu content is increased.⁸ Nickel is added to Al-Cu and Al-Si alloys to improve hardness and strength at elevated temperatures and to reduce the coefficient of expansion, as the existing Al-Si-Cu and Al-Si-Mg alloy systems lose strength above 150 °C.⁶ Several authors⁹⁻¹¹ emphasized on the importance of aluminum-copper base alloys containing additives of Mn, Mg, Ti, V and Zr, which are adapted for service at elevated temperatures, particularly such as that required in certain parts of jet engines. In addition, these alloys are characterized as high strength, high toughness, weldable, ballistic quality, castable aluminum alloys.

Manganese (Mn) is highly soluble in aluminum, so that when a casting is quenched after solution heat treatment, most of the added Mn is substantially retained in solid

Table 1. Chemical Composition of the as-Received Al-2%Cu-1%Si Alloy (wt%)

Element (wt%)					
Si	Fe	Cu	Mn	Mg	Al
1.2	0.4	2.4	0.6	0.4	Bal.

Table 2. Chemical Composition of the Alloys Used in this Study (wt%)

Alloy	Element (wt%)											
	Cu	Si	Mg	Fe	Mn	Ti	Zr	V	Ni	Cr	La	Sr
Low-Si series												
B0	2.40	1.20	0.40	0.40	0.60	0.15	0.00	0.00	0.00	0.00	0.00	0.00
B1	2.40	1.20	0.40	0.40	0.60	0.15	0.15	0.20	0.30	0.00	0.00	0.00
B2	2.40	1.20	0.40	0.40	0.80	0.45	0.15	0.20	1.00	0.2	0.20	0.015

B0 base alloy

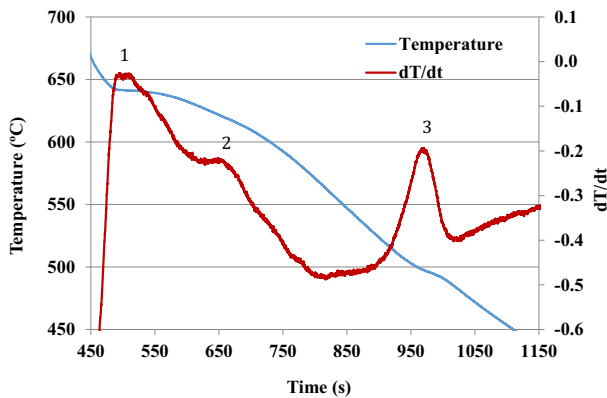


Figure 1. Solidification curve and first derivative obtained from the thermal analysis of base alloy B0.

Table 3. Proposed Main Reactions Occurring During Solidification of the Base Alloy Coded B0

Reaction	Suggested temperature (°C)	Suggested precipitated phase
1	640	Formation of α -Al dendritic network
2	620	Precipitation of α -Al ₁₅ (Fe,Mn) ₃ Si ₂
3	495	Precipitation of θ -Al ₂ Cu and Q-Al ₅ Mg ₈ Si ₆ Cu ₂

solution.¹² Manganese increases the strength of the alloy either in solid solution or by modifying the morphology of the iron intermetallic phases, which are formed after the heat treatment. Small amounts of Mn play a positive role in combining with Fe to form the Chinese script α -iron intermetallic phase instead of the platelet-like β -iron

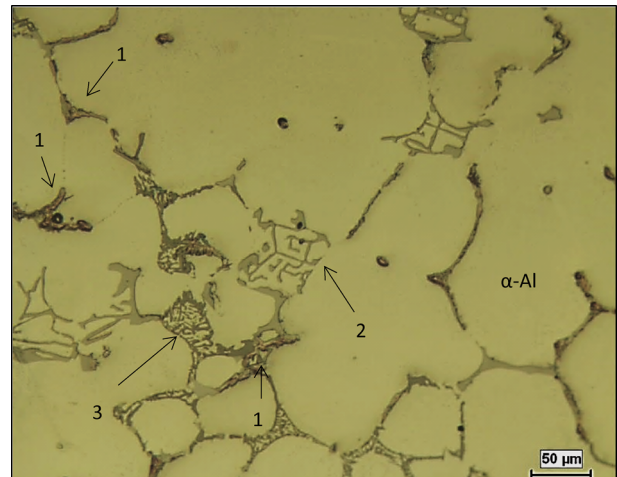
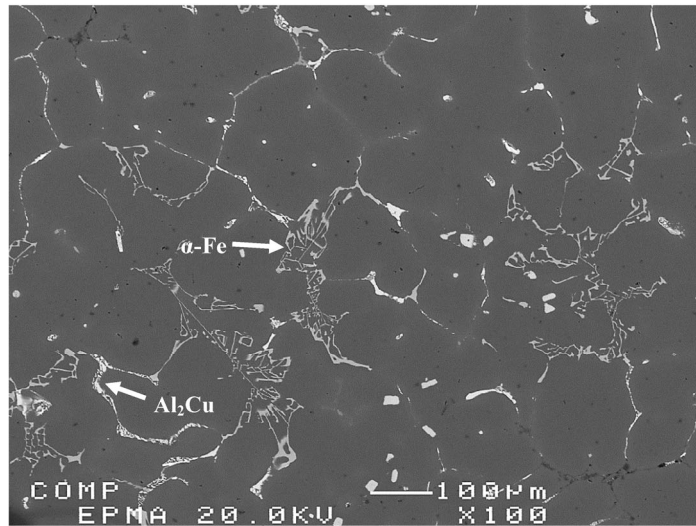


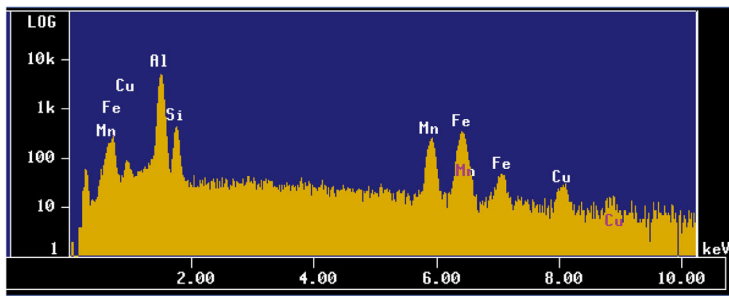
Figure 2. Optical micrograph showing the various phases formed in the base alloy B0: 1— θ -CuAl₂; 2— α -Al₁₅(Fe,Mn)₃Si₂, 3—Q-AlCuMgSi.

Al₅FeSi phase. The α -iron Al₁₅(Fe,Mn)₃Si₂ phase is much more compact and less detrimental to the mechanical properties.

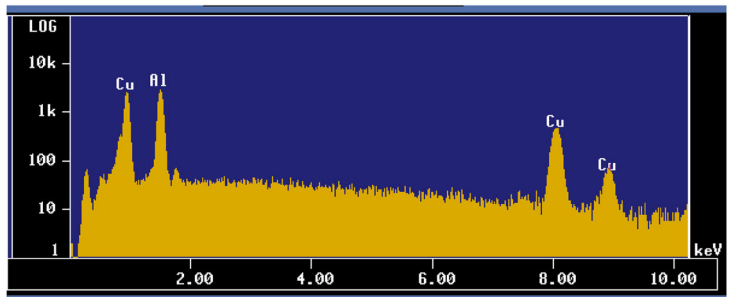
Zirconium (Zr) is usually contained in aluminum alloys in an amount of 0.1–0.25 wt%. Segregations of the Al₃Zr phase are finer in size than those of the Mn aluminides (10–100 nm).¹² Sepehrband et al.¹³ studied the effects of the addition of 0.15% Zr on the aging behavior of 319 alloy; they found that Al₃Zr precipitates are formed through the decomposition of an Al(Zr) supersaturated solid solution during solution heat treatment at 503 °C. These precipitates strengthen the matrix and provide the stable hardening response under solution heat treatment for an extended length of time. Robson and Prangnell,¹⁴ in their study of dispersoid precipitation in Zr-containing aluminum alloys, concluded that the dispersoid



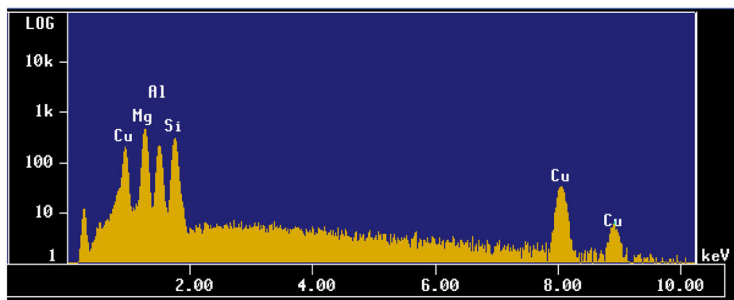
(a)



(b)



(c)



(d)

Figure 3. (a) Backscattered electron image of B0 alloy, (b–d) EDS spectra corresponding to α -Fe, Al_2Cu and Q-phase, respectively.

precipitation will only be thermodynamically possible if the Zr concentration is greater than about 0.01 wt% at 350 °C which increases to over 0.08 wt% at 500 °C.

Also, Ni and Zr when added to Al–Si alloys precipitate in the form of Al₃Ni and Al₃Zr, respectively. Vanadium (V) is added to aluminum alloys in order to increase grain refining during solidification due to the formation of the Al₁₁V intermetallic phase.¹⁵ Earlier researches studied the effect of adding vanadium to aluminum alloys and proved that traces of V in such alloys improve the mechanical properties, in particular the alloy strength,^{16,17} and enhance its plasticity behavior. According to Oak Ridge National Laboratory,¹⁸ in response to the need for low-density, high-performance alloys for use in the components of airframes and turbine engines, for example, concerted efforts have been made in recent years to improve the properties of intermetallic alloys, especially alloys based on aluminides (e.g., TiAl, Ti₃Al, NiAl, Ni₃Al, FeAl, Fe₃Al). Their inherent oxidation resistance and retention of strength at high, homologous temperatures make them prime candidates for use at intermediate temperature ranges, where creep resistant alloys are required.

Lanthanum (La) and cerium (Ce) or rare earth elements in Al alloys interact preferentially with other elements to form

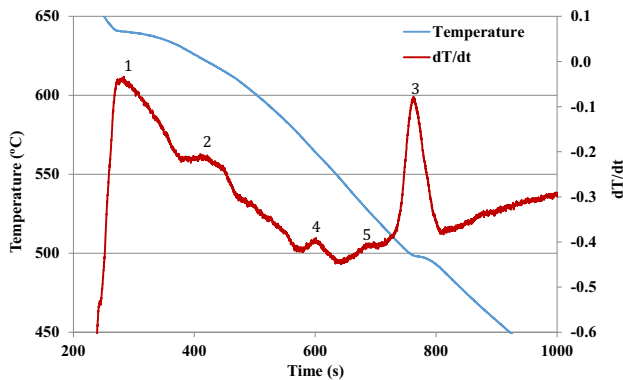


Figure 4. Cooling curve and first derivative obtained from the thermal analysis of Alloy B1.

Table 4. Proposed Main Reactions Occurring During Solidification of Alloy B1

Reaction	Suggested temperature range (°C)	Suggested precipitated phase
1	640	Formation of α -Al dendritic network
2	620	Precipitation of α -Al ₁₅ (Fe,Mn) ₃ Si ₂
3	495	Precipitation of θ -Al ₂ Cu and Q-Al ₅ Mg ₈ Si ₆ Cu ₂
4, 5	570–530	Zr- and V-rich phases

intermetallic compounds, which concentrate in the grain boundary regions and result in hindering grain boundary movement by slip. As a result, the strength of the alloy is improved at elevated temperatures. Sharan and Prasad¹⁹ investigated the influence of rare earth fluorides in hypoeutectic Al–7.5%Si alloy and reported that the tensile strength increased by 36% and the percentage elongation by about 2–3 times its original value due to the addition of up to 0.2% rare earth fluorides to the alloy. Ravi et al.²⁰ found that the addition of mischmetal up to 1 wt% results in an increase in the tensile properties and hardness by up to 20% in Al–7Si–0.3Mg alloy. This increase is attributed to the refinement of the microstructure and the formation of intermetallic compounds between Al and Si, Mg, Fe, Ce and La.

The present study was performed on Al–2%Cu–1%Si alloy which is a low-Si, low-Cu version of 319 alloy, patent # US 8,980,021 B2. The main task was to investigate the influence of the addition of different elements (Ti, Zr, V, Ni, Mn and La) on the types of intermetallics that would precipitate at low solidification rate ~ 0.35 °C/s. These elements constitute the major alloying elements that are normally used in cast alloys. We found previously that silicon can interfere with some peritectic reactions and chose a level of silicon that could still form the intermetallic phases found in 319 alloys but was less prone to disrupt the formation of aluminide phases during solidification. These elements are a mixture of transition metals and rare earth metals. Their combination represents a small fraction of the possible number of combinations but gives some insight into various combinations of additions expected to form stable dispersoids during solidification. Thermal analysis was the main tool for obtaining the solidification curves, whereas the precipitated phases were identified using optical and EPMA techniques.

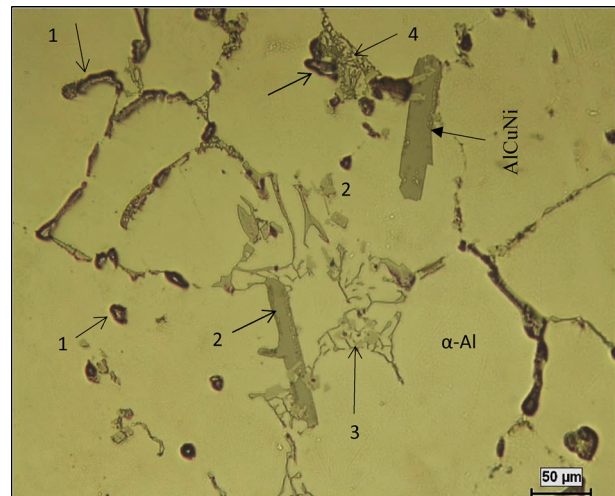


Figure 5. Optical micrograph showing the phases formed in Alloy B1: 1—Al₂Cu; 2—Zr-rich phase; 3— α -Al₁₅(Fe,Mn)₃Si₂; 4—Q-AlCuMgSi.

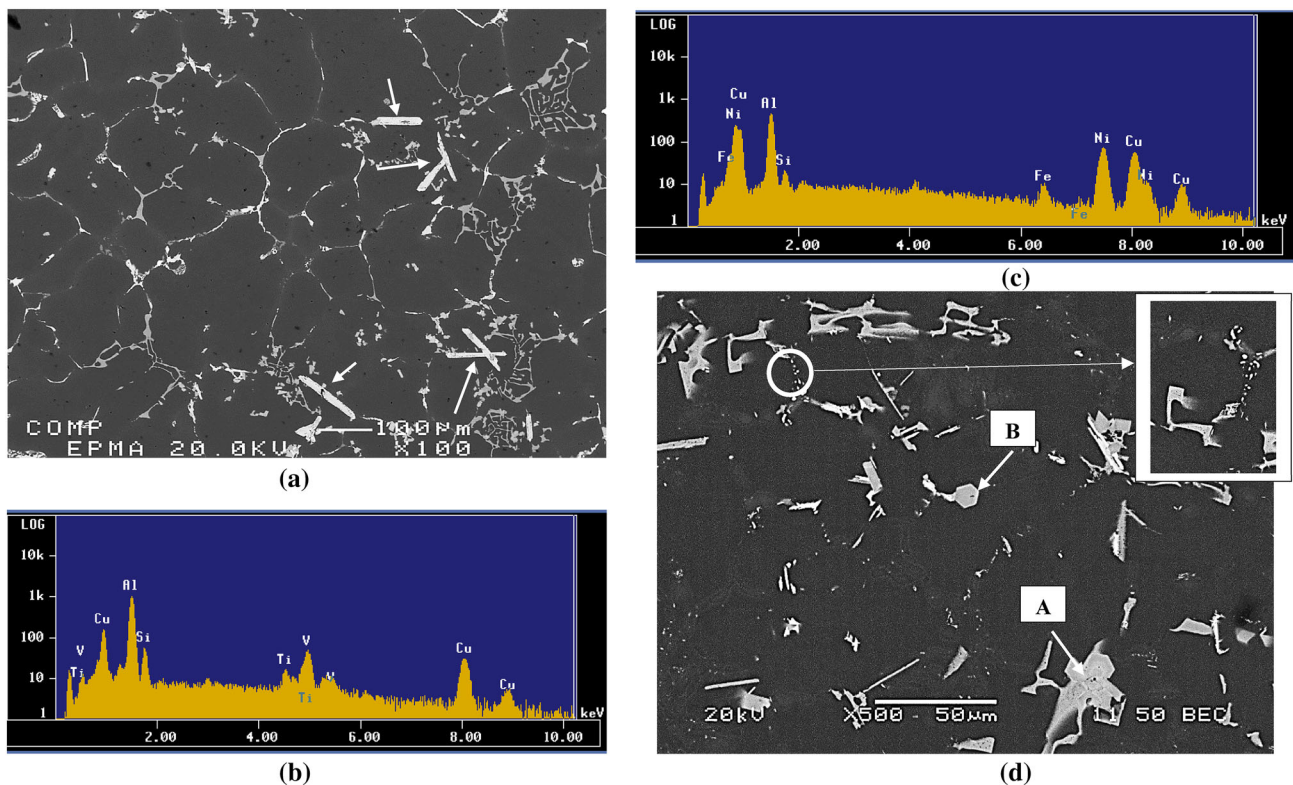


Figure 6. (a) Backscattered electron image revealing the increase in intermetallics in the aluminum matrix, (b, c) EDS spectra corresponding, respectively, to A1VCu and A1NiCu, (d) backscattered electron image of AlZrTi (bright phase-marked A) coexisting with Q-phase (gray phase-marked B)—note the precipitation of fine Al₃Zr in the circled area, (e) high-magnification electron micrograph of the Zr-rich phase-marked X in (d), revealing its star-like form, (f) EDS spectrum corresponding to area marked A in (d) mainly AlZrTi, (g) X-ray distribution of Zr dispersoids in (d).

Experimental Procedure

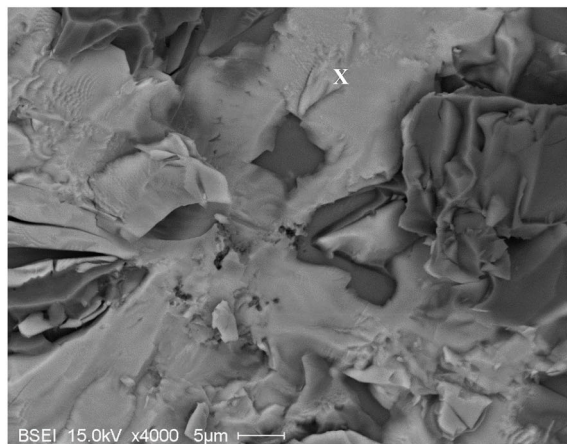
The composition of the as-received Al–2%Cu–1%Si alloy used to prepare the alloys investigated in this study is shown in Table 1. The alloy was grain-refined using Al–5%Ti–1%B master alloy to achieve a Ti level of 0.15 wt%. Other alloys were prepared from this grain-refined alloy, considered as the base alloy, by adding Sr, Ni, Zr, V, Cr and La to the base alloy melt, individually or in different combinations, to produce three alloy compositions. These alloys were coded B0 (base alloy), B1 and B2; Table 2 shows the details of the additions made in each case. All alloying elements were added in the form of master alloys.

In order to obtain the cooling curves and to identify the main reactions and corresponding temperatures occurring during the solidification of these alloys, thermal analysis of the alloy melt compositions was carried out. The melting was done in a cylindrical graphite crucible of 2-kg capacity, using an electrical resistance furnace. The melting temperature was maintained at 780 °C, while the alloys were grain-refined using Al–5%Ti–1%B using master alloy. Additions of Ni, Zr, V, Mn, La and Sr were carried

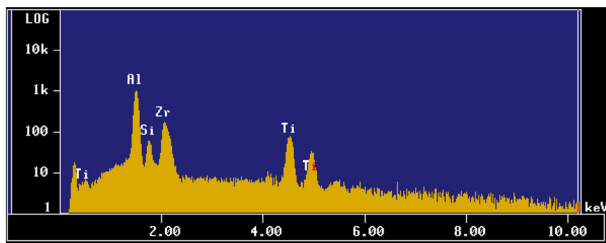
out using Al–20%Ni, Al–20%Zr, Al–15%V, Al–20%Cr, Al–15%La and Al–10%Sr master alloys, respectively.

For determining the reactions taking place during solidification, part of the molten metal was also poured into an 800-g capacity graphite mold preheated to 650 °C so as to obtain near-equilibrium solidification conditions (at a cooling rate of 0.35 °C/s). A high-sensitivity type K (chromel–alumel) thermocouple, insulated using a double-holed ceramic tube, was attached to the center of the graphite mold. The temperature–time data were collected using a high-speed data acquisition system linked to a computer system that recorded the data every 0.1 s. From these data, the cooling curves and the corresponding first derivative curves for a number of selected alloys were plotted to identify the main reactions occurring during solidification with the corresponding temperatures; the various phases which constituted the microstructure of each alloy were expected to be revealed as well.

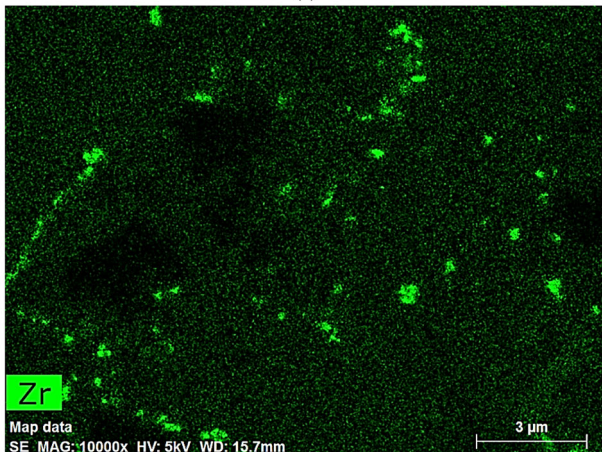
The techniques used for identifying the intermetallic phases involved using an optical microscope Clemex Vision PE4 image analysis system and an electron probe



(e)



(f)



(g)

Figure 6. continued

microanalyzer (EPMA) in conjunction with a wavelength-dispersive spectrometer (WDS), for which a JEOL JXA-8900L WD/ED Combined Microanalyzer operating at 20 kV and 30 nA with an electron beam size of $\sim 2 \mu\text{m}$ was employed. The surface fraction of the intermetallic phases was quantified using the same instrument, with special built-in software based on phase brightness where the brightness of each phase is a function of its average atomic number. The atomic number of the phase measured must be greater than that of the aluminum matrix (i.e., greater than 13).

In order to support the results obtained from the thermal analysis, DSC runs were carried out on the same alloys

(melting and solidification) at the rate of $10 \text{ }^\circ\text{C/s}$. The DSC plots are presented collectively in the [Appendix](#) section at the end.

Results and Discussion

Alloy B0

The base alloy (B0) contains 2.4% Cu, 1.2% Si, 0.4% Mg, 0.4% Fe, 0.6% Mn and 0.15% Ti. Thus, it may be classified as an Al–Cu based alloy, so that the main phases expected for this alloy will be restricted to Cu-rich intermetallic phases as well as Fe-rich intermetallic phases. In order to determine the main intermetallic phases and their formation reactions in the base alloy, thermal analysis of the B0 alloy melt was carried out under low solidification rate conditions ($\sim 0.35 \text{ }^\circ\text{C/s}$). Based on the temperature–time data obtained, the cooling curve and its first derivative were plotted, as shown in Figure 1. The numbers on the first derivative curve correspond to the same reaction numbers as those listed in Table 3.

As shown in Figure 1, Alloy B0 starts to solidify at $640 \text{ }^\circ\text{C}$ (Reaction #1) through the development of the α -Al dendritic network, followed by the precipitation of α -iron $\text{Al}_{15}(\text{Fe},\text{Mn})_3\text{Si}_2$ at $620 \text{ }^\circ\text{C}$ (Reaction #2), and then, Al_2Cu and $\text{Al}_5\text{Mg}_8\text{Si}_6\text{Cu}_2$ precipitate simultaneously as the final reaction at $495 \text{ }^\circ\text{C}$ (Reaction #3). Figure 2 shows the possible morphologies of these intermetallic phases; the α -iron $\text{Al}_{15}(\text{Fe},\text{Mn})_3\text{Si}_2$ phase appears in compacted Chinese script form which is gray in color, while the Al_2Cu phase may appear either in eutectic form (Al + Al_2Cu) or as block-like particles which appear to have a pinkish color when viewed under the optical microscope. The Q-phase, $\text{Al}_5\text{Mg}_8\text{Si}_6\text{Cu}_2$, appears in the form of small particles which are dark gray in color and growing out of the Al_2Cu phase.

Figure 3a shows the backscattered electron image corresponding to Figure 2, revealing the presence of the intermetallics confirmed by the corresponding EDS spectra displayed in Figures 3b–d.

Alloy B1

The cooling curve for Alloy B1 (B0 + 0.15wt% Zr + 0.20wt% V + 0.3wt% Ni) obtained from the temperature–time data and its first derivative plot are shown in Figure 4. The numbers on the first derivative curve correspond to the reaction numbers listed in Table 4. Apart from the α -Al dendrites and the eutectic Al_2Cu particles observed in the interdendritic regions, other phases may also be observed, as depicted in the optical micrograph of Alloy B1 shown in Figure 5. It is interesting to note that the eutectic Al_2Cu particles in Figure 5 appear similar to those shown in Figure 4 for the base alloy B0. The β -Fe

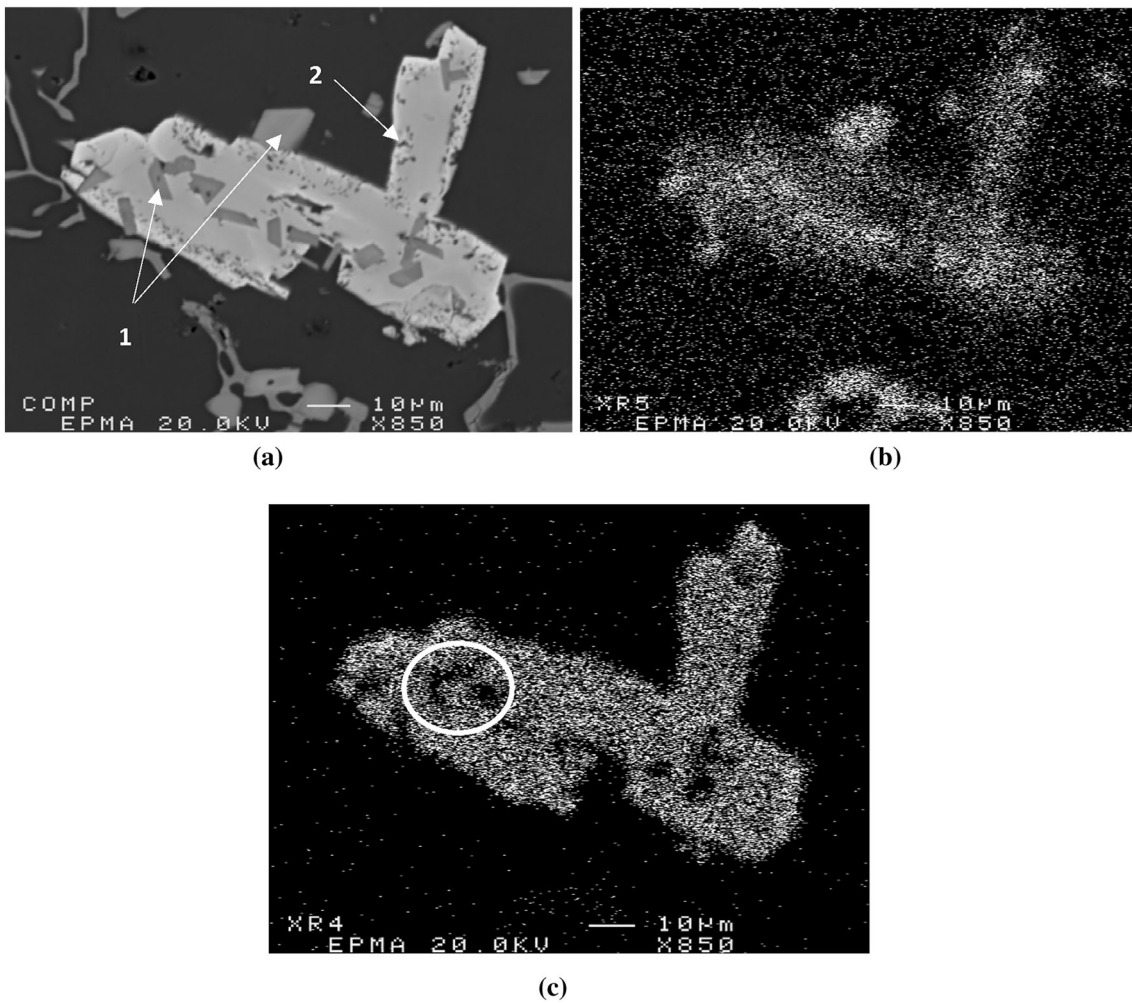


Figure 7. (a) High-magnification backscattered electron micrograph of V- and Zr-containing precipitates, (b, c) X-ray images of the distribution of (c) V and (d) Zr, in (a).

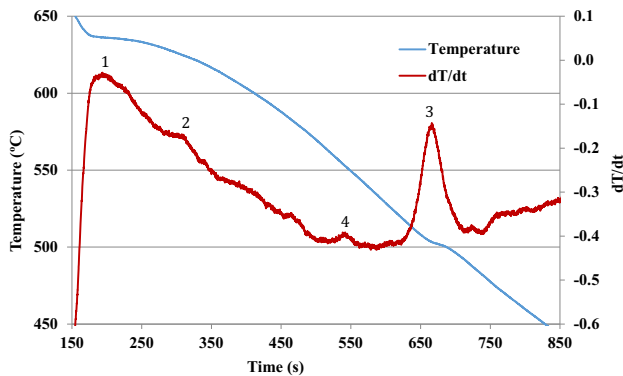


Figure 8. Cooling curve and first derivative obtained from the thermal analysis of Alloy B2.

phase is mostly associated with an alloy Fe content of more than 0.1 wt%.²¹ Increasing the Fe content to more than 0.1 wt% will increase the quantity and size of the β -phase platelets in the microstructure, which is not favorable to the mechanical properties.^{21–23} At more than 0.1 wt% Fe, however, most of the β -phase will precipitate at a higher

Table 5. Proposed Main Reactions Occurring During Solidification of Alloy B2

Reaction	Suggested temperature range (°C)	Suggested precipitated phase
1	639	Formation of α -Al dendritic network
2	615	Precipitation of α - $\text{Al}_{15}(\text{Fe}, \text{Mn})_3\text{Si}_2$
3	497	Precipitation of θ - Al_2Cu and $\text{Q-Al}_5\text{Mg}_8\text{Si}_6\text{Cu}_2$
4, 5	570–530	Zr- and V-rich phases

temperature; such β -phase platelets are characterized by their large size in the microstructure, as shown in Figure 3. It should be noted that the listed phases were identified based on WDS and EDS analyses, and with reference to the atlas of Backerud et al.²⁴

Figure 6a shows the backscattered electron image corresponding to Figure 5 revealing the presence of a large

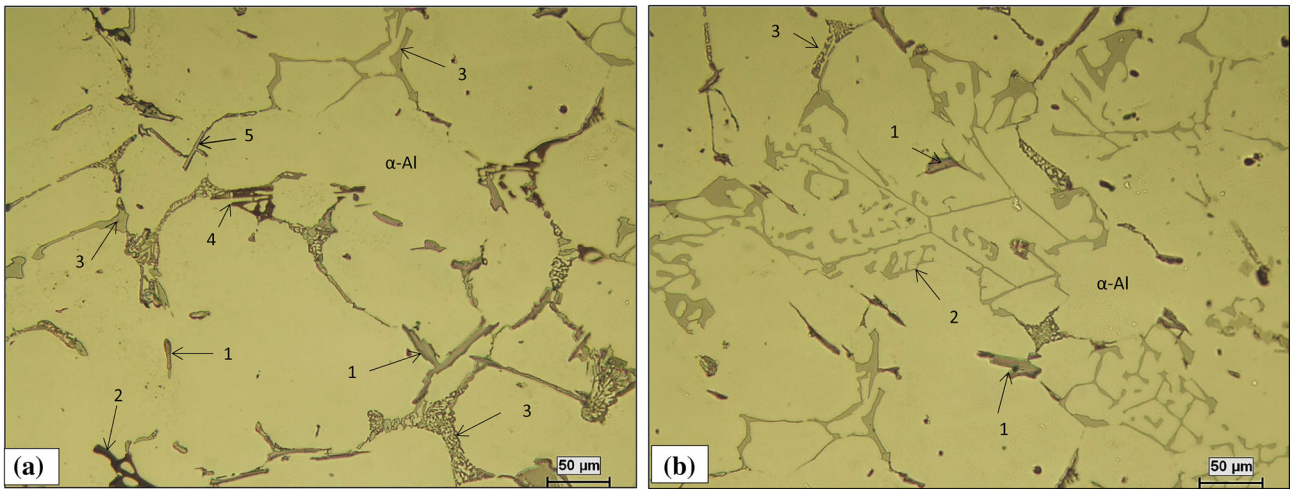


Figure 9. Optical micrographs showing the phases formed in Alloy B2: (a) 1-Al₂Cu.

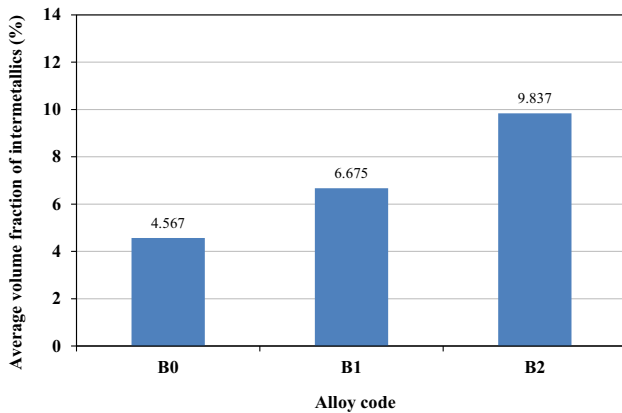


Figure 10. Average intermetallic volume fractions observed in the three alloys studied.

number of intermetallic phases. From the associated EDS spectra, it clear that both V (Figure 6b) and Ni (Figure 6c) have a strong affinity to react with the Cu in the alloy. However, this is not the case for Zr (Figure 6d and e) that

tends to react, rather, with Ti. In all cases, however, the Si concentration is low. The white arrows in Figure 6a indicate the precipitation of Al–Cu–Ni compound in the form of short platelets.

Figure 7a shows a high-magnification backscattered electron image taken from Figure 6a revealing the possibility of the precipitation of V-rich particles on the surface of the Zr-rich phase. Apparently there is a limited solubility of V in Zr as inferred from (i) the gray color of the V-rich phase particles (atomic no. 23) compared to the lighter color of the Zr phase (atomic no. 40) as shown in Figure 7b-c and (ii) the presences of cavities in the X-ray Zr map—see the white circled area in Figure 7c.

Alloy B2

The cooling curve of Alloy B2 (B0 + 0.80% Mn + 0.20% La + 0.20% Cr) was obtained from its temperature–time data and is shown along with its first derivate plot in Figure 8. The reactions taking place during solidification for

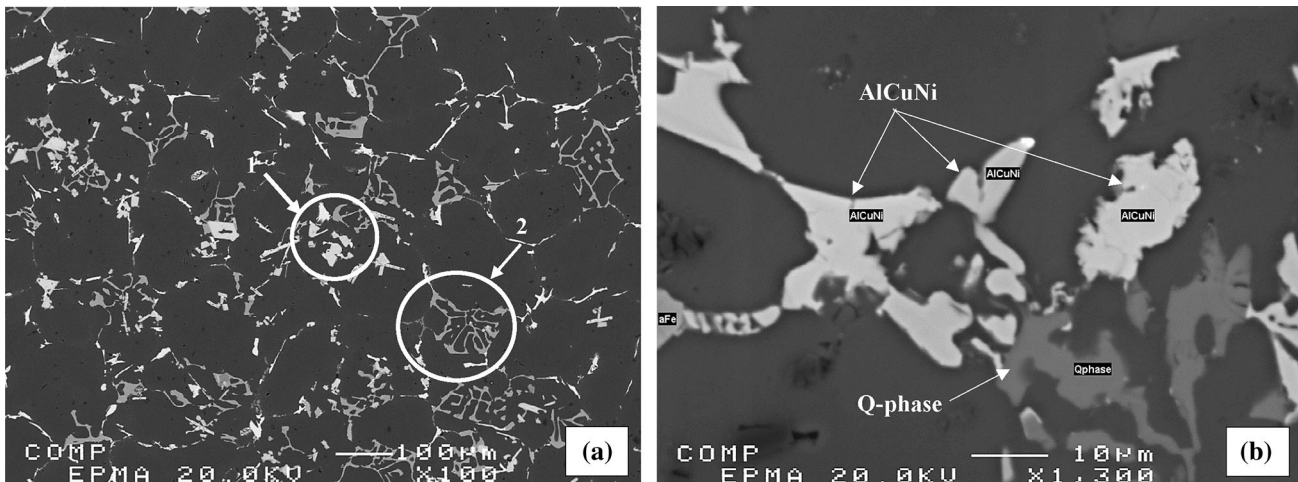


Figure 11. Backscattered electron images from B2 alloy: (a) low magnification, (b) high magnification.

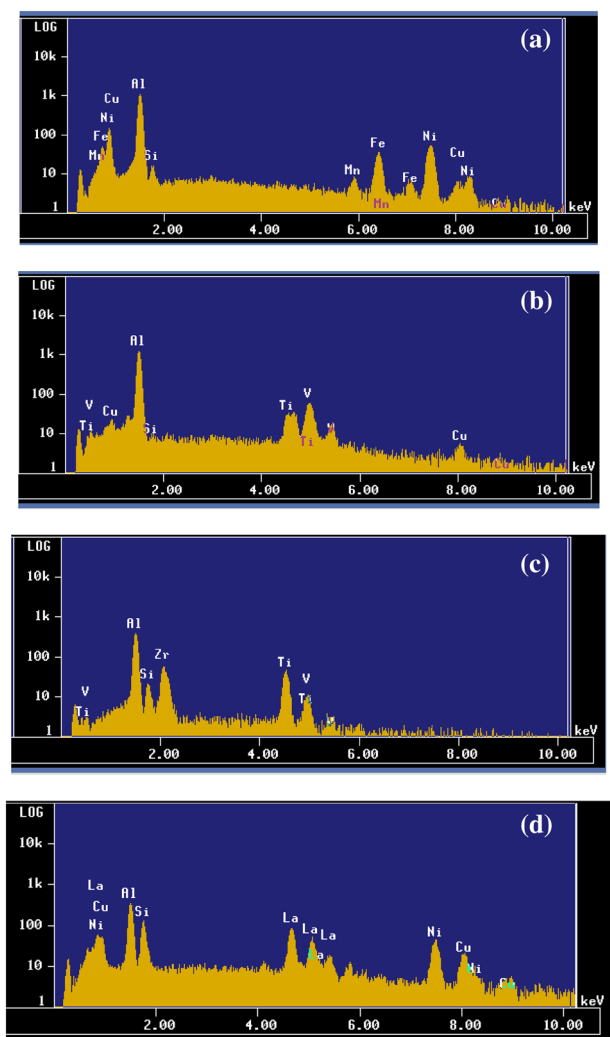


Figure 12. EDS spectra showing precipitation of different transition and rare earth metal-based compounds.

this alloy are listed in Table 5. Similarities between the solidification curves of Alloys B1 and B2 are noted. Apart from the α -Al dendrites and the eutectic Al_2Cu particles observed in the interdendritic regions, other phases observed in the optical micrograph include the α -Fe or $\text{Al}_{15}(\text{Fe},\text{Mn})_3\text{Si}_2$ script phase, the Q-AlCuMgSi phase, Mg_2Si phase in black script form and the AlSiTiZrV phase, as shown in Figure 9. Neutralization of the harmful effects of iron through the promotion of the less harmful α -Fe Chinese script phase rather than the brittle needle-like β -Fe phase is sought with the goal of improving strength, ductility and other properties.^{9,11}

In the alloys containing nickel, the Al_3CuNi phase is observed situated adjacent to the Al_2Cu phase and both phases are located at the limits of the dendritic α -Al phase; this observation is in agreement with the fact that the reactions noted in the thermal analysis curves, namely Reactions #4 and #5, are contiguous to one another.¹⁶

Since the B2 alloy contains maximum alloying elements (Ni, Mn and La), it is expected to show relatively higher density of intermetallics compared to those obtained from B0 and B1 alloys as shown in Figure 10.

Figure 11a displays the backscattered electron image corresponding to Figure 9, revealing intermetallics containing Ni (marked 1) and Mn (marked 2). The high-magnification image shown in Figure 11b illustrates the precipitation of massive AlCuNi phase particles near or at the Q-phase.

Figure 12 exhibits a series of EDS spectra corresponding to the different phases observed in Figure 11a. Based on these spectra, it should be noted that although Figure 12c reveals the presence of peaks corresponding to V and Zr, this may not necessarily be the result of a V-Zr interaction, but could possibly be caused by the precipitation of particles of two phases on top of each other, as demonstrated in Figure 7. Since the accelerating voltage is 20 kV, the electron beam could easily penetrate both particles depending on their thickness. Figure 12d illustrates the possibility of interaction between the transition and rare earth metals used in this alloy.

To further examine the hypothesis of a V-Zr interaction, Figure 13 shows the distribution of different elements in a cluster of particles observed in the backscattered electron image or captured picture (CP) of Figure 13a, which show clearly that V and Zr are not mixed together. In this context, the added grain refiner or TiB_2 particles—circled in white in Figure 13c—could act as nucleation sites for these V- and Zr-containing intermetallics.

Table 6 summarizes the possible intermetallics observed in the present alloys based on WDS analysis. Figure 14 displays the interaction between rare earth metals (La in this case) and transition metals (Cu- and V-rich phases) as confirmed from the associated EDS spectrum shown in Figure 14e. In addition, V has a limited interaction with other transition elements to form the α -Fe phase. Figure 14 also reinforces the observation that there is no interaction between V and Zr.

Concluding remarks

From the analysis and discussion of the results presented in this article, the following conclusions may be drawn.

1. The thermal analysis experiments provide evidence of the reactions taking place during solidification under close-to-equilibrium cooling conditions.
2. The θ - Al_2Cu , Q- $\text{Al}_5\text{Mg}_8\text{Si}_6\text{Cu}_2$ and the Chinese script-like α - $\text{Al}_{15}(\text{Fe},\text{Mn})_3\text{Si}_2$ phases were identified as the main microstructural constituents of the base alloy B0.

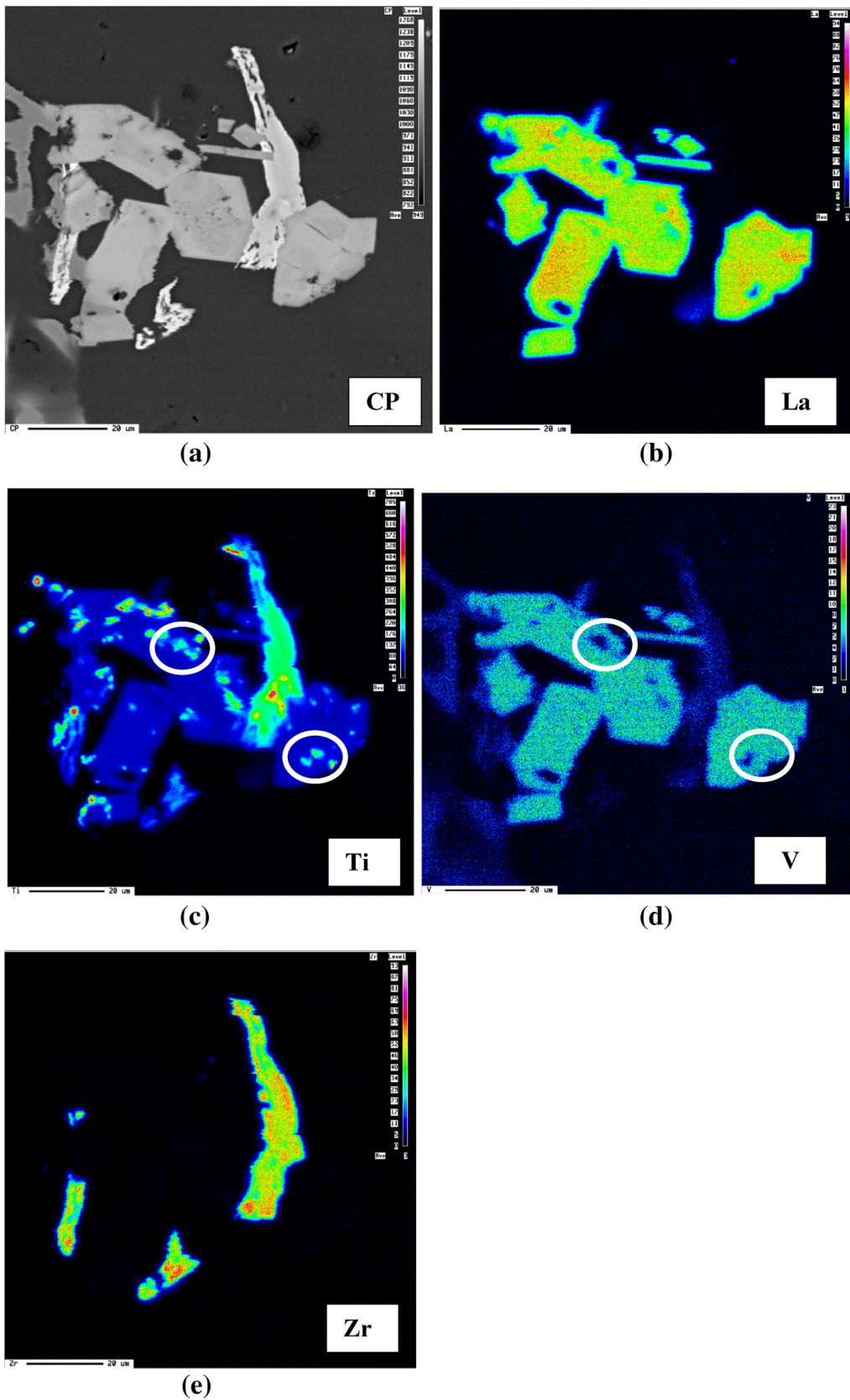


Figure 13. (a) Backscattered electron image, (b-e) X-ray images showing distribution of La, Ti, V and Zr in (a).

Table 6. Chemical Analysis of Intermetallics Observed in the Present Study (at.%)

Alloy	Ni	Al	Zr	Ti	Fe	Cu	Mg	Cr	Mn	Si	La	V	Calculated formula
B0	0.05	63.48	0.00	0.20	13.02	2.15	0.12	0.00	12.22	8.67	0.00	0.00	Al _{14.6} (Fe,Mn,Cu) _{6.3} Si ₂
B0	0.00	48.17	0.00	0.15	0.01	51.68	0.12	0.00	0.00	0.19	0.00	0.00	Al _{0.9} Cu
B0	0.15	13.83	0.00	0.15	0.01	20.74	36.42	0.00	0.00	29.06	0.00	0.00	Al _{1.3} Mg _{3.5} Si _{2.8} Cu ₂
B1	0.014	71.95	12.94	7.39	0.01	0.07	0.03	0.016	0.19	4.77	0.00	2.61	* Al _{15.1} (Zr,Ti) _{4.3} Si
B1	0.08	82.72	0.47	1.92	0.04	2.87	1.93	0.028	0.03	1.65	0.00	8.24	** Al _{14.9} (Cu,V) ₂
B1	0.00	71.09	12.33	7.58	0.01	0.05	0.00	0.024	0.176	5.33	0.00	1.38	Al _{13.3} (Zr,Ti) _{3.7} Si
B1	15.66	61.92	0.07	0.00	0.45	21.45	0.00	0.008	0.033	0.35	0.00	0.03	Al _{7.9} Cu _{2.7} Ni ₂
B1	0.04	82.48	0.48	1.44	0.01	3.185	2.08	0.00	0.006	1.91	0.00	8.36	Al _{14.3} (Cu,V) ₂
B1	0.44	75.50	0.00	0.01	8.70	0.83	0.02	0.01	6.55	7.41	0.004	0.50	Al _{10.2} (Fe,Mn) _{2.1} Si
B1	0.06	82.00	0.41	1.32	0.00	2.87	2.12	0.00	0.00	1.30	0.742	7.77	Al _{15.4} (Cu,V) ₂
B1	16.73	61.82	0.01	0.03	0.30	21.00	0.00	0.00	0.01	0.06	0.00	0.04	Al _{7.4} Cu _{2.5} Ni ₂
B2	11.14	81.05	0.01	0.00	4.95	0.96	0.13	0.00	0.60	1.13	0.008	0.005	Al _{3.7} Fe _{0.4} Ni
B2	18.13	61.71	0.01	0.00	0.11	19.90	0.00	0.01	0.03	0.09	0.00	0.00	Al _{3.4} Cu _{1.1} Ni
B2	0.016	83.21	0.18	2.40	0.02	0.93	1.11	0.27	0.034	0.36	4.86	6.14	Al _{17.1} (V,Ti) _{1.8} La
B2	0.026	70.74	13.33	9.27	0.02	0.07	0.00	0.11	0.11	5.05	0.00	0.007	Al _{14.0} (Zr,Ti) _{4.5} Si
B2	0.031	82.46	0.14	2.52	0.02	2.10	1.59	0.57	0.05	0.42	4.83	5.86	Al _{17.1} (V,Ti) _{1.8} La
B2	0.45	51.5	0.15	0.00	4.85	0.45	19.5	0.01	0.05	23.12	0.00	0.01	Al ₈ Mg ₃ FeSi ₆
B2	0.04	71.78	11.77	9.82	0.01	0.10	0.00	0.11	0.105	4.79	0.004	0.47	Al _{14.0} (Zr,Ti) _{4.5} Si
B2	0.04	62.23	0.012	0.18	14.25	0.10	0.00	6.46	11.5	4.79	0.004	0.47	Al _{26.0} (Fe,MnCr) _{13.4} Si ₂

Bold values are to facilitate calculating the formulas of the phases listed in the last column, based on the elements present in these phases

* Trace elements

** Traces of Mg₂Si

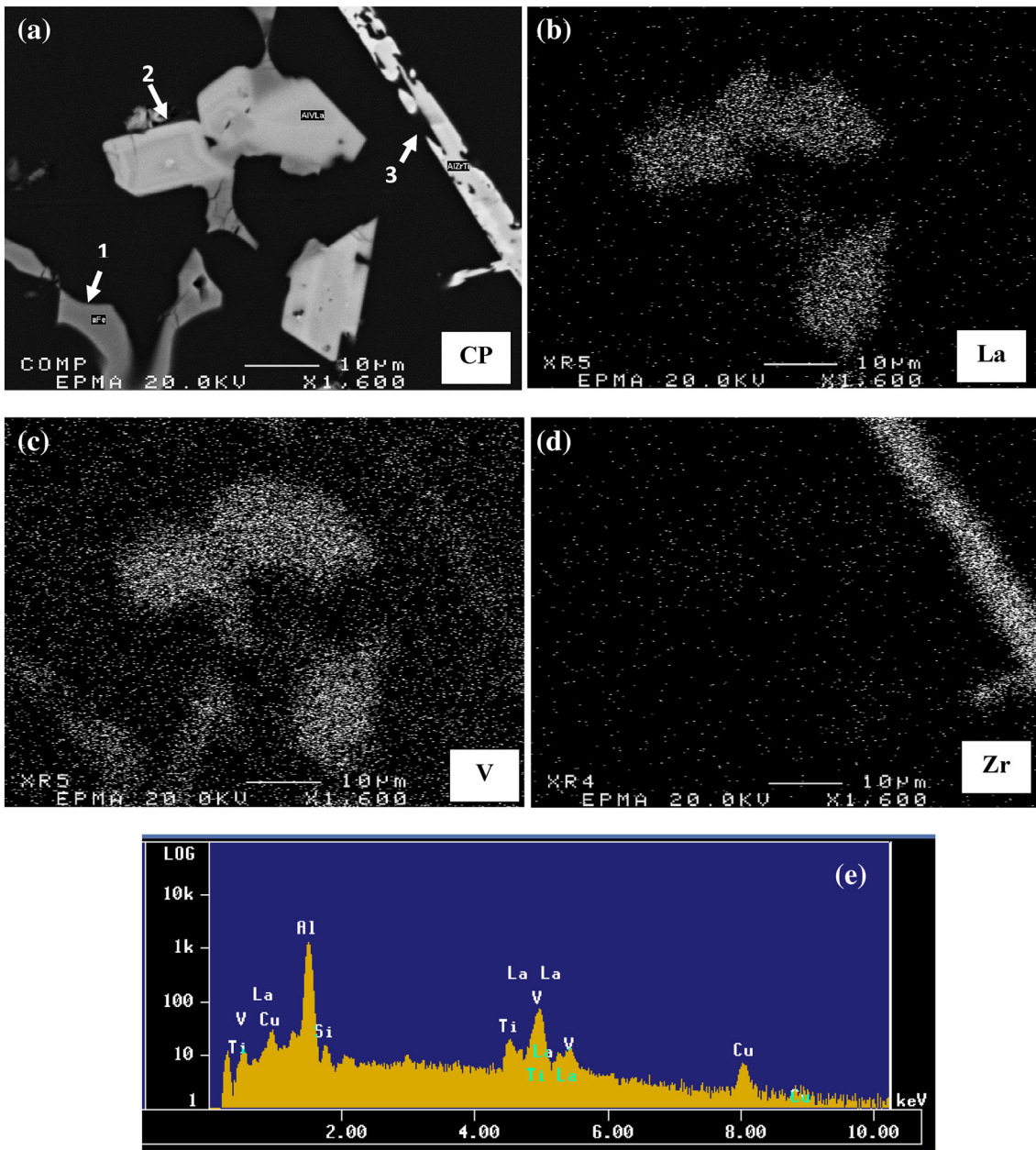


Figure 14. (a) Backscattered electron image showing 1— α -Fe, 2—AlVCuLa, 3—AlZrTi phases, (b–d) X-ray images of La, V and Zr distribution in (a), (e) EDS spectrum taken from AlVCuLa phase in (a).

3. Nickel and V react with Cu, Fe, Zr and La, resulting in the formation of complex compounds. Vanadium, however, shows no affinity to react with Zr.
4. The addition of Mn (0.8 wt%) and Cr (0.2 wt%) in Alloy B2 helped in reducing the detrimental effects of the platelet morphology of the β -iron Al_3FeSi phase by replacing it with the more compact and hence less detrimental α - $\text{Al}_{15}(\text{Fe},\text{Mn})_3\text{Si}_2$ Chinese script phase and sludge particles (α - $\text{Al}_{15}(\text{Fe},\text{Mn},\text{Cr})_3\text{Si}_2$).

Acknowledgements

The authors would like to thank Amal Samuel for enhancing the quality of the images and figures used in this article. The authors also would like to extend their thanks to Aluminum Technology Centre—Chicoutimi—for running the DSC analysis tests.

Appendix

See Figures 15 and 16.

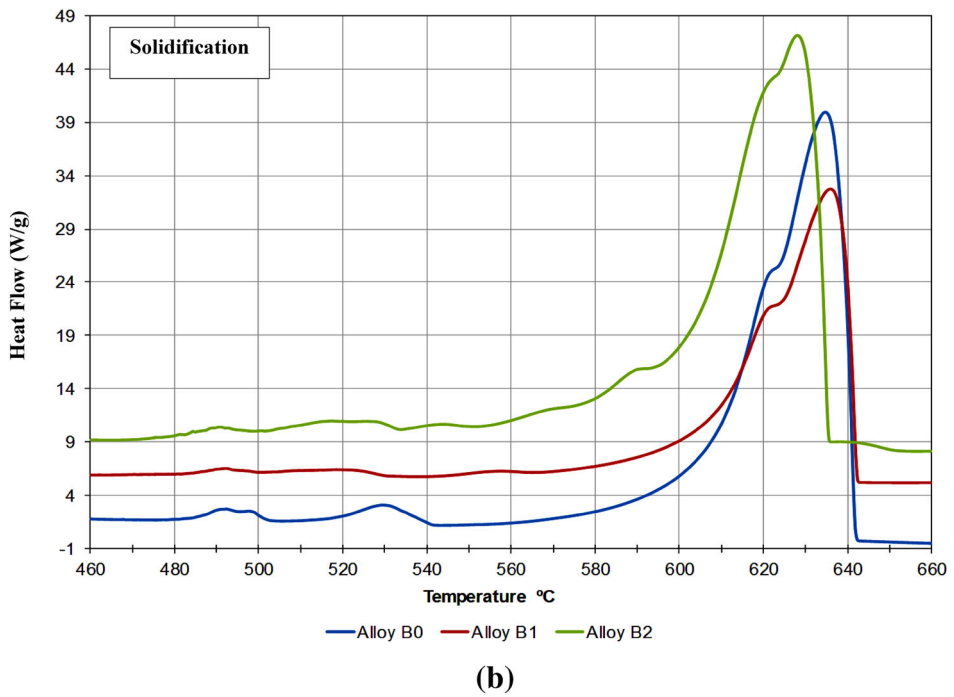
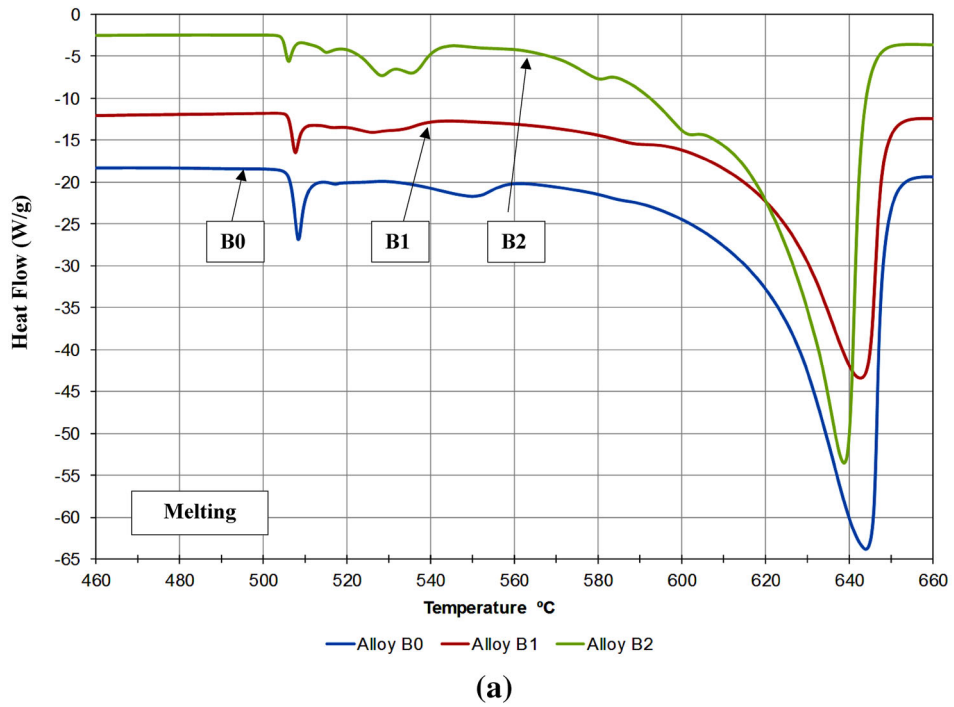
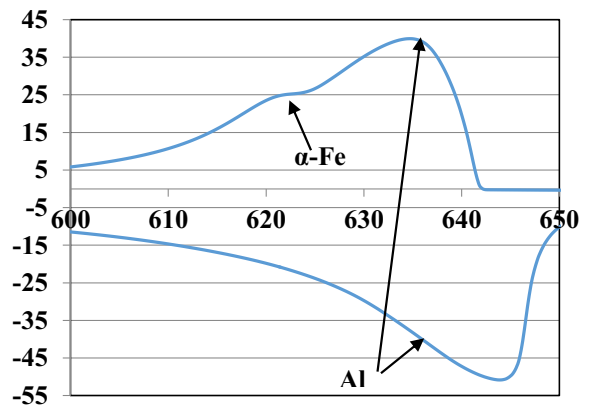
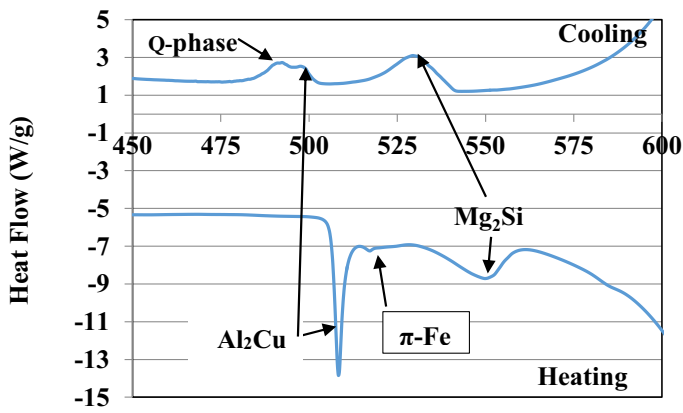
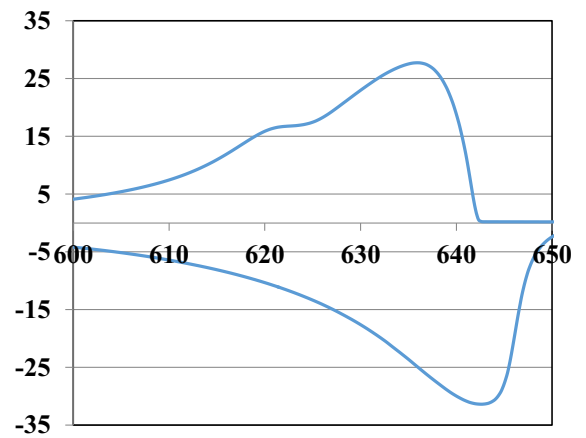
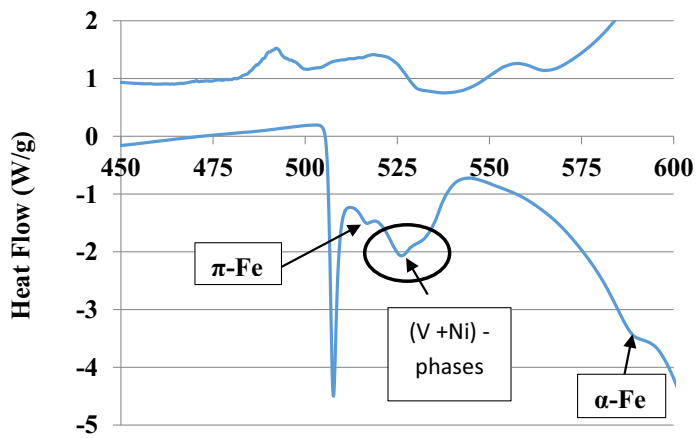


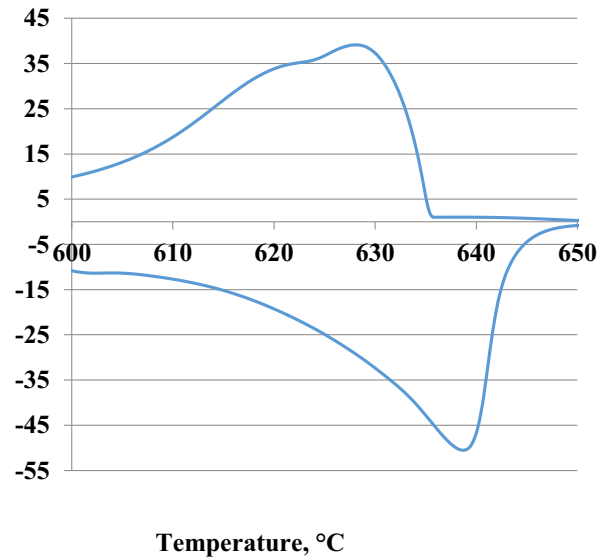
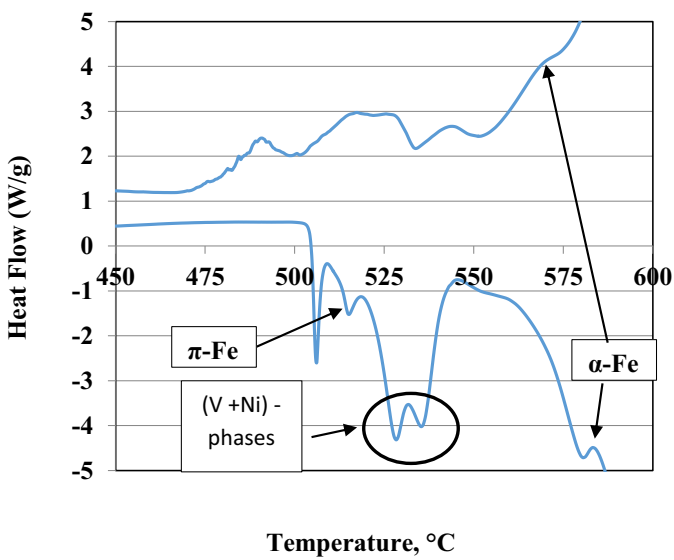
Figure 15. DSC runs of the three alloys superimposed: (a) melting, (b) solidification.



(a)



(b)



(c)

◀ **Figure 16. Enlarged views of the DSC runs of: (a) B0, (b) B1, (c) B2 alloys. Notes: 1—Reduction in the energy for melting of the Al₂Cu phase with the increase in the Ni content, i.e., 15 W/g in the case of B0 versus 5 W/g for B2 alloy. 2—The energy associated with the precipitation of each individual intermetallic is too small (less than 2 W/g) which makes it difficult to identify the precipitation temperature of each phase precisely. 3—It is not possible to carry out in situ quench since all peaks occur in a narrow temperature range.**

REFERENCES

1. D.A. Granger, W.G. Truckner, E.L. Rooy, Aluminum alloys for elevated temperature application. Trans. American Foundrymen's Society, vol. 94, 86–143, 1986 (8 pages)
2. E.L. Rooy, A history of aluminum foundry alloy development. In: Proceedings from the AFS International Conference on Structural Aluminum Casting, 2–4, November 2003, Orlando, FL P 87–98, 2003 (12 p)
3. D.J. Weiss, G.A. Gegel, K.S. Sadayappan, Development of cast Al alloys for elevated temperature (250 °C) service. Transactions of the American Foundry Society, vol. 119, Paper No. 11-017, 43–48
4. C.R. Loper, T.E. Prucha, Feed metal transfer in Al–Cu–Si alloys, Transactions of the American Foundrymen's Society, vol. 98, Paper 90–165, 845–853, 1990 (9 p)
5. P. Ouellet, F.H. Samuel, Effect of Mg on the ageing behaviour of Al–Si–Cu 319 type aluminium casting alloys. J. Mater. Sci. **34**(19), 4671–4697 (1999)
6. F.J. Tavitias-Medrano, H.W. Doty, S. Valtierra, F.H. Samuel, On the enhancement of the impact toughness of A319 alloys: role of Mg content and melt treatment. Int. J. Metalcast. **11**(3), 536–551 (2017)
7. S. Seifeddine, S. Johansson, I.L. Svensson, The influence of cooling rate and manganese content on the β -Al₅FeSi phase formation and mechanical properties of Al–Si-based alloys. Mater. Sci. Eng., A **490**(1–2), 385–390 (2008)
8. A.M.A. Mohamed, F.H. Samuel, A.M. Samuel, H.W. Doty, Influence of additives on the impact properties of Al–10.8%Si near-eutectic Al–Si alloys. Mater. Des. **30**(10), 4218–4229 (2009)
9. B.C. Crinar, Aluminum base alloy, US Patent No. 2,706,680 (1955)
10. High strength weldable aluminum base alloy product and method of making same, US Patent 4610733 (1986)
11. A. Druschitz, High strength, high toughness, weldable, ballistic quality, castable aluminum alloy, heat treatment for same and articles produced from same, US Patent 11/270,767 (2005)
12. V.I. Elagin, Ways of developing high-strength and high-temperature structural aluminum alloys in the 21st century. Metal Sci. Heat Treat. **49**(9–10), 427–434 (2007)
13. P. Sepehrband, R. Mahmudi, F. Khomamizadeh, Effect of Zr addition on the aging behavior of A319 aluminum cast alloy. Scr. Mater. **52**, 253–257 (2005)
14. J.D. Robson, P.B. Prangnell, Dispersoid precipitation and process modelling in zirconium containing commercial aluminum alloys. Acta Mater. **49**, 599–613 (2001)
15. S.C. Bergsma, M.E. Kassne, X. Li, in 3rd *International Conference on Processing and Manufacturing Advanced Mater.*, U.S. Department of Energy, Inc., 2000, pp. 12–17
16. S.C. Bergsma, M.E. Kassne, The new aluminium alloy AA6069. Mater. Sci. Forum **217–222**, 1801–1806 (1996)
17. F.J. MacMaster, K.S. Chan, S.C. Bergsma, M.E. Kassner, Aluminum alloy 6069 part II: fracture toughness of 6061-T6 and 6069-T6. Mater. Sci. Eng., A **289**, 54–59 (2000)
18. Oak Ridge National Laboratory Intermetallics Program." National Research Council, *Intermetallic Alloy Development: A Program Evaluation* (The National Academies Press, Washington, DC, 1997). <https://doi.org/10.17226/5701>
19. R. Sharan, N.P. Saksena, Rare earth additions as modifiers of aluminum silicon alloys. AFS Trans. **3**(1), 29–33 (1978)
20. K.R. Ravi, R.M. Pillai, K.R. Amaranathan, B.C. Pai, M. Chakraborty, Fluidity of aluminum alloys and composites: a review. J. Alloys Compd., **456**, 201–210 (2008)
21. M. Tash, F.H. Samuel, F. Mucciardi, H.W. Doty, Effect of metallurgical parameters on the hardness and microstructural characterization of as-cast and heat-treated 356 and 319 aluminum alloys. Mater. Sci. Eng., A **443A**, 185–201 (2007)
22. Z. Ma, A.M. Samuel, F.H. Samuel, H.W. Doty, S. Valtierra, A study of tensile properties in Al–Si–Cu and Al–Si–Mg alloys: effect of β -iron intermetallics and porosity. Mater. Sci. Eng., A **490**(1–2), 36–51 (2008)
23. Z. Ma, A.M. Samuel, F.H. Samuel, H.W. Doty and S. Valtierra, Effect of iron and cooling rate on tensile properties of B319.2 alloys in non-modified and Sr-modified conditions, in *Transactions of the American Foundry Society*, vol. 112, 131–140, 2004
24. L. Bäckerud, G. Chai, J. Tamminen, *Solidification Characteristics of Aluminum Alloys*, vol. 2 (AFS/Skanaluminum, USA, 1990), p. 255